Published in final edited form as:
Anat Rec (Hoboken). 2008 February ; 291(2): 204–215. doi:10.1002/ar.20631.

Connexin 43 Expression Delineates Two Discrete Pathways in the Human Atrioventricular Junction

WILLIAM J. HUCKER[1], **MEGAN L. McCAIN**[1], **JACOB I. LAUGHNER**[1], **PAUL A. IAIZZO**[2], and **IGOR R. EFIMOV**[1,*]

[1]Washington University, Saint Louis, Missouri

[2]University of Minnesota, Minneapolis, Minnesota

Abstract

Gap junction expression has been studied in the atrioventricular junction (AVJ) of many species, however, their distribution in the human AVJ is unknown. The AVJ expression of the gap junction protein connexin 43 (Cx43) is species dependent; therefore we investigated its distribution in the human AVJ. Using Masson trichrome histology, we reconstructed the AVJ of three normal human hearts and one with dilated cardiomyopathy in three dimensions. Cx43 was immunolabeled with vimentin and α-actinin to determine the cellular origin of Cx43 and was quantified in the following structures: interatrial septum (IAS), His bundle, compact node (CN), lower nodal bundle (LNB), leftward and rightward nodal extensions (LE and RE), and inferior, endocardial, and left-sided transitional cells. Histology revealed two nodal extensions in three of four hearts. Cx43 was found in the myocytes, but not fibroblasts, of the AVJ. LE and CN Cx43 was lower than the IAS ($P < 0.05$) and the RE, LNB, and His all expressed Cx43 similarly, with approximately half of IAS expression (RE: 44 ± 36%; LNB: 50 ± 26%; His: 48 ± 12%, P = NS compared with IAS). Cx43 levels in transitional cells were similar to the IAS (P = not significant). Cx43 was found in myocytes of the human AVJ, and its expression pattern delineates two separate continuous structures: one consists of the LE and CN with little Cx43, and the other consists of the His, LNB, and RE expressing approximately half the Cx43 of the IAS. The differential Cx43 expression may provide each structure with unique conduction properties, contributing to arrhythmias arising from the AVJ.

Keywords

atrioventricular node; dual-pathway electrophysiology; connexin43; slow pathway; AVNRT; fibroblasts

Detailed investigations of the atrioventricular junction (AVJ) in many animal models have demonstrated the enormous complexity of this structure in terms of cell and tissue morphology, functional characteristics, and protein distribution. While many histological studies have investigated the human AVJ, and clinical electrophysiological studies have provided a substantial amount of information regarding AVJ function in vivo, the number of molecular investigations of the human AVJ is very limited because of the inherent difficulty of procuring human tissue in a timely manner (Davis et al., 1995). Nevertheless, such studies are vitally necessary to the basic understanding of clinically relevant phenomena, such as atrioventricular nodal reentrant tachycardia (AVNRT) and AV block, and to increase the understanding of

*Correspondence to: Igor R. Efimov, Department of Biomedical Engineering, Washington University in St. Louis, MO 63130. Fax: 314-935-8377. igor@wustl.edu.

variables such as age, which are difficult to address in animal models. In addition, interspecies differences in protein expression patterns can limit the extrapolation of animal data to the human (Coppen and Severs, 2002; Coppen et al., 2003). Therefore, human molecular studies are crucial because expression patterns in the human AVJ should become the framework in which studies from animal models are interpreted.

Several tissue types are involved in atrial-His conduction, and the term AVJ is used in this study to encompass them all (Billette, 2002). Proximally, the specialized conduction tissue of the AVJ consists of the inferior nodal extensions, which extend from near the coronary sinus (CS) ostium to the node itself (Inoue and Becker, 1998). Previously, these extensions were termed “posterior” rather than “inferior” (Inoue and Becker, 1998; Dobrzynski et al., 2003); however, when the heart is oriented anatomically, these extensions actually run inferior to the CN and, therefore, we use the term “inferior nodal extension” in this study (Cosio et al., 1999). The inferior nodal extensions merge to become the AV node (AVN), which then penetrates the central fibrous body to become the His bundle (Tawara, 1906). Connecting the AVN and nodal extensions to the surrounding atrial tissue are transitional cells that can be divided into three groups based on their location relative to the AVN: endocardial transitional cells contact the AVN on its endocardial aspect, left-sided transitional cells approach the AVN from the left side of the interatrial septum (IAS), and inferior transitional cells approach the AVN near the coronary sinus ostium (Anderson and Ho, 2000, 2002).

To accommodate its complex physiological role, the AVJ has developed very heterogeneous gap junction expression, with more types of gap junctional proteins expressed in the AVJ than anywhere else in the heart. Specifically, four cardiac connexins have been described to date (Cx43, Cx40, Cx45, and Cx30.2/31.9), and each of these proteins has been found in animal studies of the AVJ (Boyett et al., 2006). Cx43 and Cx40 are both associated with rapidly conducting cardiac tissues (with Cx40 having a higher conductance than Cx43), and Cx45 and Cx30.2/31.9 are associated with slowly conducting tissues (Boyett et al., 2006). The expression patterns of these connexins in the AVJ are very speciesdependent: rat hearts do not express Cx43 or 40 in the AVJ, however, rabbits express both (Coppen and Severs, 2002; Dobrzynski et al., 2003). Only one study has documented the expression of connexins in the human AVJ to our knowledge (Davis et al., 1995), where they found that Cx43, Cx40, and Cx45 were all present, yet this study did not survey where in the AVJ each connexin was expressed.

Traditionally, connexins have been assumed to form gap junctions between two adjacent myocytes. However, recent publications also suggest that functional gap junctions are formed between myocytes and fibroblasts (Camelliti et al., 2005), possibly by means of Cx43 coupling (Goldsmith et al., 2004). In this study, we investigated Cx43 expression throughout the various tissues of the AVJ, as well as whether Cx43 forms gap junctions between myocytes and fibroblasts. We correlated Cx43 immunofluorescence with three-dimensional (3D) reconstructions of the AVJ constructed from Masson trichrome histology, showing that Cx43 expression pattern delineates domains of the AVJ (not apparent with histology) that may have functional consequences.

METHODS

The use of human hearts for research was approved by the Institutional Review Boards at Washington University and the University of Minnesota. Three specimens were provided by the Upper Midwest Organ Procurement Organization (LifeSource, St. Paul, MN; they also provided preapproval for this protocol); these hearts were deemed nonviable for transplantation. An additional specimen was a transplant recipient’s explanted heart with idiopathic dilated cardiomyopathy (DCM). The clinical data that are known regarding each specimen is shown in Table 1. These specimens were placed in frozen tissue-embedding

medium (Histo Prep^{TM}, Fisher Scientific, Fair Lawn, NJ) and stored in a −80°C freezer at the University of Minnesota, before being shipped on dry ice to Washington University. Subsequently, they were thawed at 4°C before dissection. The triangle of Koch was exposed, and an approximately 4 × 4cm^2 area of tissue at the apex of the triangle of Koch was dissected (Fig. 1A) and re-frozen at −80°C. The tissue blocks were cryosectioned at 16 μm, mounted on Superfrost Plus glass slides (Fisher Scientific), and stored at −80°C until use. The location of each tissue section was documented throughout the sectioning process.

3D Reconstruction

To create a 3D reconstruction of the AVJ, tissue sections approximately 0.5–1.0 mm apart (Fig. 1B) were stained with Masson trichrome. Histology sections were photographed with a × 2 lens, and a mosaic image of the tissue section was created. The image of each section was imported into Rhinoceros NURBS modeling for Windows version 3.0 (Robert McNeel & Associates) and outlined to separate areas of: fat as well as any imbedded strands of transitional cells, IAS/transitional cells, ventricular septum, connective tissue (central fibrous body, mitral and tricuspid valves), conduction system (His bundle, compact AV node, lower nodal bundle, rightward and leftward inferior nodal extensions), and major arteries and veins (Fig. 1C). Transitional cells were incorporated into the areas of the IAS or the fatty tissue surrounding the conduction system because the transitional cell boundary was difficult to define and quite irregular, which made 3D reconstruction of transitional cells confusing and unclear. However, in Figure 1C, arrows point to transitional cells that lie within the fatty tissue, and arrowheads point to transitional cells from the left atrium. The set of derived outlines from each section was rotated and aligned to those of the previous section. The correct 3D placement of each section was determined by using distances recorded during tissue cryosectioning. Figure 1D shows the resultant correctly aligned and positioned outlines for the conduction system in the explanted heart from the patient with DCM. For each tissue type, the set of outlines was lofted to create a mesh approximating the 3D volume (Fig. 1E), which was then rendered to create a solid 3D volume (Fig. 1F).

Immunohistochemistry

For immunohistochemistry, tissue sections were first fixed, permeabilized, and blocked by immersion in 3.7% formaldehyde for 5 min, 0.15% Triton for 15 min, and 10% normal horse serum for 60 min. Using immunohistochemistry, we visualized three different proteins: the gap junctional protein Cx43; the myocyte marker α-actinin, which is expressed in the sarcomeres of myocytes; and the intermediate filament protein vimentin, which is expressed in the cytoskeletal intermediate filaments of fibroblasts and endothelial cells (Camelliti et al., 2005). In cardiac tissue, endothelial cells are present in blood vessels, whereas fibroblasts are present throughout the myocardial tissue. Therefore, fibroblasts can be differentiated from endothelial cells based on location in the tissue, and we used this marker to visualize fibroblasts in the myocardium. The following primary antibodies were applied overnight at 4°C: rabbit anti-Cx43 (Sigma, 1:1,000), mouse anti—α-actinin (sarcomere specific, Sigma, 1:1,600), and guinea pig anti-vimentin (Progen, 1:800). The following secondary antibodies were applied for 2 hr at room temperature: Alexa Fluor 555 goat anti-rabbit IgG (Molecular Probes, 1:800), Alexa Fluor 488 goat anti-mouse IgG_1 (Molecular Probes, 1:800), and Alexa Fluor 647 goat anti-guinea pig IgG (Molecular Probes, 1:800). Immunofluorescent studies in human cardiac tissue can be quite difficult due to autofluorescence (Billinton and Knight, 2001); therefore, sections were immersed in a 1% Sudan Black (Sigma) solution for 10 min (Schnell et al., 1999) to reduce autofluorescence originating from lipofuscin particles found in human tissue. Tissue sections were subsequently mounted with ProLong Gold antifade reagent with 4′,6-diamidine-2-phenylidole-dihydrochloride (DAPI; Invitrogen).

Connexin Quantification

Confocal immunohistochemical images were collected using a ×40 lens and individual images were pieced together to create a mosaic image at three different planes within the AVJ. The first plane was a section through the inferior nodal extensions, the second plane was through the compact AV node (CN), and the third plane was through the His bundle. In the first plane, Cx43 was quantified in the leftward inferior nodal extension, rightward extension, inferior transitional cells, and the IAS. In the second plane, Cx43 was quantified in the CN, lower nodal bundle (LNB), endocardial transitional cells, left atrial transitional cells, and the IAS. Finally in the third plane, Cx43 was quantified in the His bundle and the IAS. Connexin densities within the various regions of the tissue were determined using a custom program (MATLAB, Mathworks, Natick, MA). A full description of the algorithm has been published previously (Hucker et al., 2007a) and is provided in the online data supplement. Briefly, the mosaic image of the area of interest was thresholded twice to produce two black and white images of the Cx43 channel. The first threshold selected positive Cx43 staining in the image. The second threshold was much lower than the first and selected any tissue in the image. The area of each was corrected, and the Cx43 area was divided by the tissue area to give a percentage of the tissue area that corresponded to Cx43 staining (see online data supplement).

Colocalization

Colocalization plots were used to determine which cell types expressed Cx43. In a three-channel, 3D confocal Z-stack, each voxel has three intensity values, one each for red, green, and blue staining. A colocalization plot, generated with Volocity (Improvision, Inc., Lexington, MA), displays two of these intensity values as a function of each other. By definition, two proteins are highly colocalized in a particular volume when fluorescence intensities corresponding to these two proteins are high in the voxel corresponding to this volume. Therefore, if two proteins are colocalized in many voxels, the colocalization plot will contain a significant diagonal distribution. Voxels with the highest degree of colocalization will be displayed in the upper-right quadrant. In contrast, if the two proteins are not colocalized, the colocalization plot shows voxel values near each axis, with no diagonal elements present.

Statistics

Cx43 quantification data are represented as mean ± standard deviation. Cx43 levels were compared using the nonparametric Kruskal-Wallis test (MATLAB). A value of $P < 0.05$ was considered statistically significant.

RESULTS

Cx43 Expression in the Conduction System

For one representative AVJ preparation, Masson trichrome histology, Cx43 immunofluorescence, and the 3D reconstruction of the preparation is shown in Figures 2–4. Inferiorly, the AVN begins as the inferior nodal extensions, which vary both in length and number (Inoue and Becker, 1998). In three of the four hearts in this study, there were two inferior nodal extensions, while the other had only one. The preparation shown in Figures 2–4 possessed both a leftward and rightward extension: the leftward extension begins near the left side of the IAS, whereas the rightward extension lies adjacent to the septal leaflet of the tricuspid valve (Fig. 2A). While the rightward extension expressed Cx43 (Fig. 2E,F), there was virtually no Cx43 present in the leftward extension (Fig. 2D). In this preparation, the rightward extension was located in close proximity to layers of inferior transitional cells, which also expressed Cx43 (Fig. 2E,F). Transitional cells were found closely related to the rightward extension in three of four preparations. Additionally, large veins were observed in close proximity to the rightward extension in each preparation, as seen in Figure 2A—C. Between

the leftward extension and the rightward extension, there was a variable amount of Cx43 negative tissue, which was continuous with the compact AVN superiorly (Fig. 2C). The amount of this tissue varied between preparations. Throughout Figure 2, it is clear that fibroblasts are interspersed between the myocytes of the rightward and leftward extensions, as shown with vimentin staining (blue). The 3D reconstruction of this preparation is shown in Figure 2G, split open at the plane shown in Figure 2A—C to display the rightward and leftward extensions within the tissue.

Figure 3 illustrates the Masson trichrome, Cx43 expression, and 3D reconstruction of the AVN in this preparation. The AVN is bordered by the central fibrous body (CFB), a layer of fibrofatty tissue separating the AVN from atrial tissue, and by thin layers of endocardial transitional cells as seen in Figure 3A. On the posterior aspect of the AVN, transitional cells which connect the left side of the IAS to the AVN make contact with AVN tissue. Many strands of transitional cells also lie within the fibrofatty tissue layer; however, these strands of tissue were not outlined separately in the reconstruction.

The AVN can be divided into the CN and the LNB based on functional and morphological characteristics (Anderson et al., 1974; Billette, 2002). The CN is composed of small densely packed irregularly shaped cells, whereas the LNB cells are larger and oriented parallel to each other. We observed a consistent heterogeneity in Cx43 expression between these two structures. The LNB, which occupies the anterior portion of the AVN, closest to the ventricle, expressed more Cx43 than the posterior CN region, closest to the atrium (Fig. 3B,C,G). Inferiorly, the CN was continuous with the leftward extension, and the LNB was continuous with the rightward extension. Therefore, the CN and leftward extension were outlined as one continuous structure in the reconstruction. Likewise, the rightward extension and LNB were reconstructed as a single volume (Fig. 3H). Both sets of transitional cells that are visible in this section, the left sided and the endocardial transitional cells, expressed high levels of Cx43, similar to the IAS (Fig. 3D,E). As can be seen in Figure 3, an extensive network of fibroblasts was present around the myocytes of the conduction system in the entire AVN region (Fig. 3B,F,G).

Figure 4 displays the His bundle of this preparation. The His bundle is completely surrounded by the fibrous tissue of the CFB, as seen in both the histology and the 3D reconstruction (Fig. 4A,E). The proximal end of the His bundle was defined as the point where the AVN was completely surrounded by the CFB, which was the transition point suggested by Tawara between the AVN and the His bundle (Tawara, 1906). The His bundle was reconstructed from this point to the point where it joined the ventricular septum.

Cx43 was heterogeneously expressed throughout the His bundle, as seen in Figure 4B,C. In this example, a higher level of Cx43 expression is seen on the endocardial and ventricular aspects of the His bundle. However, this pattern was not consistent; in other preparations, Cx43 was highly expressed on the atrial border of the His bundle. Whereas Tawara's transition point between the His bundle and the AVN is convenient morphologically, we did not observe an abrupt change in Cx43 expression at the beginning of the His bundle as defined by Tawara. Instead Cx43 expression gradually changed from the CN/LNB pattern seen in the AVN to the pattern shown in the His bundle. As can be seen in Figure 4B,D, a large number of fibroblasts are also present in the His bundle surrounding most of the His bundle myocytes.

Even though an extensive network of fibroblasts was present throughout the AVJ, as seen in Figures 2–4, we found that the overwhelming majority of Cx43 was solely expressed within the myocytes, with exceedingly few examples of Cx43 within fibroblasts or between myocytes and fibroblasts. Figure 5 displays maximum projection images of two representative, high resolution 3D confocal image stacks where α-actinin, vimentin, and Cx43 were labeled. Using

the method of colocalization plots, we determined the cellular origin of Cx43 in each voxel. In Fig. 5A—C, data recorded from the LNB are displayed. The maximum projection image illustrates that fibroblasts surround the myocytes; however, Cx43 is expressed solely within and between the myocytes. In Fig. 5B, a colocalization plot illustrates the red and green intensity values of each voxel within the volume imaged. The voxels that had high green intensities (i.e., specific Cx43 staining) were spread across the values of the α-actinin axis, indicating that Cx43 staining was present in voxels which also expressed α-actinin. In Fig. 5C, a colocalization plot of the blue and green intensity values from the same volume is displayed. In this plot, the voxels of specific Cx43 staining are clustered along the Cx43 axis, indicating that specific staining of Cx43 only occurred in voxels with no blue intensity. In fact, of the 14,490 voxels in this particular volume that were in the upper half of Cx43 intensity, only 1 voxel was also in the upper half of vimentin intensity. Figure 5D—F illustrates the same pattern of Cx43 expression in the CN. In the CN, there is much less Cx43 than in the LNB (Fig. 3); however, the colocalization plots in Fig. 5E and F indicate that whatever Cx43 is expressed in the CN is within or between myocytes, with very few voxels of specific Cx43 staining having any blue intensity. In this volume, 34 of the 953 voxels in the upper half of Cx43 staining were also in the upper half of vimentin staining; however, these voxels were not clustered together in one location. Instead, they appeared as one or two voxels that were independent of each other. Thus, we conclude that there is very little evidence for gap junction formation between myocytes and fibroblasts in the human AVJ.

Cx43 Quantification

Cx43 was quantified throughout the various tissue types in the AVJ. For comparison, Cx43 was also quantified in the IAS in each tissue section. Cx43 expression was relatively constant between the three different groups of transitional cells and the IAS, as shown in Figure 6. When expressed as a percentage of IAS Cx43, Cx43 in the endocardial transitional cells was 112 ± 32%, 78 ± 26% in the left sided transitional cells, and 89 ± 35% in the inferior transitional cells (P = NS for each).

When Cx43 was quantified in the conduction system of each preparation, a distinct pattern emerged as shown in the bar graph in Figure 7. The rightward extension, LNB, and His bundle all expressed Cx43 similarly to each other (ratio to the IAS was 44 ± 36%, 50 ± 26%, and 48 ± 12%, respectively). Although the average Cx43 expression in each of these structures was not statistically different from the IAS due to the small number of hearts in this study, it is clear that the Cx43 expression was consistent between them. However, Cx43 expression in the leftward extension and the CN were both statistically lower than in the IAS (5 ± 4% and 12 ± 11% of the IAS signal, respectively, $P < 0.05$ for each). Cx43 expression was also statistically lower in the leftward extension and the CN than in the LNB ($P = 0.03$ and $P = 0.02$, respectively).

Conduction System Reconstruction

The 3D reconstructions of the conduction system from each heart, consisting of the leftward and rightward extensions, CN, LNB, and His bundle is shown in two views in Figure 8. Each panel shows the reconstruction of the conduction system of one heart. The left view of each panel demonstrates the orientation of the conduction system within the triangle of Koch, blood vessels located in close proximity to the conduction system, and the CFB, which encases the His bundle. The right view shows the conduction system by itself, and the three planes where Cx43 expression was quantified. The His bundle of each preparation is shown in green. The LNB and rightward extension are depicted as a continuous structure in yellow. The leftward extension and CN are shown as a continuous structure in cyan. Finally, layers of inferior transitional cells, which were closely related to the rightward extension, are shown in orange. These areas of close apposition between transitional cells and the rightward extension may be

the interface between the atrial myocardium and the nodal extension. In two preparations (Fig. 8A,B), the rightward extension was longer than the leftward extension. As seen in Figure 8C, one preparation had a rightward, but no leftward extension, and finally in the heart with DCM (Fig. 8D), the leftward extension was actually slightly longer than the rightward extension.

In the DCM heart (Fig. 8D), the IAS was much thicker than in the other three preparations, and in this heart the leftward extension protrudes prominently toward the left atrial side of the IAS (in the dorsal—ventral direction). Therefore, an additional view of the conduction system, which is rotated 90 degrees from the endocardial view shown in Figure 8A—C, is shown in D. The conduction system in the DCM heart was thicker than those of the normal hearts, as can be seen in Figure 8D. Animations of the reconstruction of the DCM heart and the normal heart in Fig. 8A are provided in the online data supplement.

DISCUSSION

In this study, we have reconstructed the 3D anatomy of the conduction system in the human AVJ and mapped the distribution and cellular origin of Cx43. Our results indicate that Cx43 is distributed heterogeneously in the myocytes of the region: the rightward extension, LNB, and His bundle express similar levels of Cx43 (approximately half the level of IAS expression), while the leftward extension and the CN express very little Cx43 as compared to the IAS.

Inoue and Becker described a series of 21 hearts where they found that 7/21 (33%) had only a rightward but no leftward extension, 13/21 (62%) had a rightward extension that was longer than the left, and 1/21 (5%) that had only a leftward extension (Inoue and Becker,1998). Our sample of hearts closely mimics those described by Inoue and Becker: two of four (50%) had a longer rightward extension than leftward, and one of four (25%) had only a rightward extension. Interestingly, in the DCM heart of our study the leftward extension was actually longer than the rightward extension, which is a variant that Inoue and Becker did not observe. Whether this variation is simply rare and did not surface in their investigations or whether it is due to the pathologic state of this sample cannot be determined from our study. It is certainly possible that the long leftward extension is related to the DCM, because the overall morphology of the conduction system was different in this heart (Fig. 1C), and it was larger than the other hearts in this study (Fig. 8D). The thickness of the IAS was also much greater in this heart than in the other hearts (data supplement movie 2); therefore, the leftward extension may have elongated preferentially in this heart as the myocardium remodeled because it was oriented in the dorsal—ventral direction. We also found that the Cx43 expression in this heart was higher than the normal hearts (Figs. 6, 7); however, a previous study demonstrated that left ventricular Cx43 expression is reduced in patients with DCM (Dupont et al., 2001). Therefore, future studies will be necessary to determine the effect of various cardiomyopathies on the AVJ.

In the study of Inoue and Becker (1998) that was entirely based upon histological investigations, no mention of the LNB was made. In part, this may be due to the fact that the LNB of the human is difficult to recognize with histology alone. In this study, we found that with the additional use of the Cx43 marker, we could consistently visualize the LNB, which indicates that morphologically similar cells and structures can possess very different molecular characteristics. Future studies will be necessary to determine whether other connexin isoforms delineate similar domains throughout the human AVJ.

The rabbit AVJ is often used as an experimental model of the human AVJ. In the rabbit, there is only one nodal extension that lies below the right atrial endocardium in the myocardial isthmus between the coronary sinus and tricuspid valve, very similar to the position of the human rightward extension. In this study, Cx43 quantification revealed two axes of Cx43 expression in the human AVJ: the rightward extension, LNB, and the His bundle all express

Cx43 similarly to each other and at higher levels than the CN and leftward extension. A previous study reported that the rabbit also has two domains of Cx43 expression. Ko et al. found that the His bundle, lower nodal cells, and the nodal extension all express Cx43 similarly and that the CN does not express detectable Cx43 (Ko et al., 2004). Therefore, it is consistent between the human and the rabbit that the rightward extension/LNB is connected to the His bundle differently than the leftward extension/CN. The similarity between the data in this study and rabbit investigations provides further evidence that the rabbit is an appropriate model of the human cardiac conduction system (Rothenberg and Efimov, 2006).

Using the method of colocalization plots, we have concluded that the interaction between fibroblasts and myocytes by means of Cx43 is minimal if any in the human AVJ (Fig. 5). The colocalization technique is useful to tease out the location of immunofluorescent signals in 3D space. It is also quantitative: it displays the values of every voxel within a stack of images, which removes any selection bias from the results. However, this technique assumes that, if fibroblasts express Cx43, the signal would be colocalized with vimentin. This assumption may or may not be correct, because vimentin is a cytosolic protein and Cx43, if expressed and functional, would be membrane bound. However, at the optical resolution used in this study, the pixel resolution of our confocal images is 240 nm in x and y (125 × 125 μm field of view with 512 × 512 pixels) and ~500 nm in z, which is quite large with respect to the separation of proteins in a cell. It seems reasonable that vimentin fibers would be expressed within 240 nm of the cell membrane, therefore, we believe that our assumption is valid. Also, the same restrictions on the physical overlap of α-actinin and Cx43 would apply because sarcomere-specific α-actinin would be expressed in the cytosol of myocytes, yet the colocalization plot indicates that there is colocalization between α-actinin and Cx43.

Functional Implications

Dual pathway electrophysiology is one of the pathological hallmarks of the human AVJ, providing the substrate for reentrant arrhythmias such as AVNRT (Moe et al., 1956). Typically, the AVJ is described as having two functional pathways, a slow and a fast pathway, which give rise to AVNRT. Anatomically, the substrate for the slow pathway involves the isthmus of myocardium between the coronary sinus and the tricuspid valve (Nikolski et al., 2003), which is ablated to treat AVNRT, and transitional cells act as the fast pathway. There is evidence that the rightward extension is the substrate of the slow pathway (Inoue et al., 1999; Medkour et al., 1998); however, it is debated whether the rightward extension, the inferior transitional cells that overlay this extension, or a combination of both, is the true substrate of the slow pathway (McGuire, 2000). If the rightward extension is indeed a substrate of the slow pathway, it is intriguing that our results indicate that the rightward extension contains a relatively large amount of Cx43, because Cx43 expression would suggest fast conduction. However, conduction velocity is not solely dependent upon Cx43 expression; Cx40, Cx45, possibly Cx30.2/31.9 (Kreuzberg et al., 2006), as well as ion channel expression will certainly affect conduction velocity in the nodal extensions. In reality, it may not be conduction time within the inferior nodal extension that is responsible for the “slow” nature of the slow pathway, but it may be the interface between the inferior transitional cells and the inferior nodal extension that is responsible for slow conduction (Nikolski et al., 2003; Hucker et al., 2007b). However, future studies correlating functional properties of the nodal extensions with the distribution of Cx40, Cx45, Cx30.2/31.9 as well as ion channel distributions will be necessary to fully understand the role of the nodal extensions in AVNRT.

We found that the probable substrate of the fast pathway, the transitional cell layers around the CN, expressed Cx43 at similar levels to the atrial septum, which would functionally support fast conduction within these cell layers. Both structurally and functionally, these cells are intermediate between the atrial myocardium and the AVN in terms of action potential

characteristics and cell morphology (Anderson and Ho, 2002; Billette, 1987). However, in terms of Cx43 expression, Figure 3C shows that instead of a smooth transition in Cx43 at the interface of the transitional cells and the CN, there is a dramatic decrease in Cx43 expression from the transitional cells to the CN, which may slow action potential propagation into the CN (Shaw and Rudy, 1997).

The role of the leftward extension/compact nodal structure is less clear. Because it expresses little Cx43, this structure would presumably conduct slowly and may provide a slowly conducting pathway in cases of AVNRT where more than one slow pathway is observed, or in intranodal reentry. Consistent with this hypothesis is the correlation between the fact that AVNRT involving multiple pathways is less common than AVNRT involving one slow pathway, and the leftward extension is inconsistently expressed in humans (Inoue and Becker, 1998). The leftward extension could also provide a slowly conducting pathway between the left atrial side of the IAS and the nodal tissue (Katritsis and Becker, 2007). Finally, inferior transitional cells come into close proximity to the leftward extension in some cases (Fig. 4A—C); therefore, a reentry circuit may possibly be sustained between the two nodal extensions and the inferior transitional cells.

The continuous expression of Cx43 from the rightward INE to the LNB and the His bundle suggests that these structures form one continuous structure and that the rightward extension is connected to the His bundle differently than the leftward extension. In the rabbit, functional studies in our lab and others have indicated that excitation spreading from the inferior nodal extension excites the His bundle differently than excitation spreading from the fast pathway (Zhang et al., 2001; Hucker et al., 2007b), and specifically that the AV delay can be avoided by pacing near the inferior nodal extension (Hucker et al., 2007b). Our data in this study suggest that the same may be true in the human with excitation in the rightward extension spreading by means of the LNB to a specific Cx43-positive domain of the His bundle, bypassing the compact AV node.

The possibility of unique coupling between the rightward extension and the His bundle opens the possibility of exploiting this connection to achieve His bundle excitation without engaging the compact AV node. Recent pacing strategies have explored alternative pacing sites, such as direct His bundle pacing, to achieve synchronized ventricular contraction (Deshmukh and Romanyshyn, 2004; Laske et al., 2006; Zanon et al., 2006). Attempting to pace the rightward extension rather than the His bundle itself would expand the area at the base of the right atrium where a pacing lead could be implanted and potentially lower pacing thresholds because the rightward extension is not encased in fibrous tissue like the His bundle.

Our 3D reconstruction of the human AVJ indicated that the tissue surrounding the conduction system is richly vascularized. The veins surrounding the AVJ are large, with diameters ranging from 0.29–0.56 mm in the 4 AVJs we reconstructed. Because the coronary sinus is located very close to the AVJ, the veins shown in the 3D reconstructions of Figure 8 either join the coronary sinus very near its os, or drain into the right atrium directly. Although CS os access can be challenging in some patients (Hill et al., 2006), it may soon be possible to navigate these veins with catheters for ablations, pacing, or localized pharmacologic delivery (e.g., to achieve AVN modulation during atrial fibrillation) without the tissue damage induced by an active lead screwed into the myocardium (Sigg et al., 2006).

Conclusions

Our study presents for the first time the mapping of Cx43 in the human AVJ. We have found that the conduction system in the human AVJ expresses two domains with respect to Cx43 density: the rightward extension, LNB, and His bundle all express Cx43 similarly to each other, while the leftward extension and the CN possess very little Cx43. These two separate domains

may, therefore, possess unique conduction properties that contribute to heterogeneous conduction and supraventricular arrhythmias arising from the AVJ.

Limitations

Our study was limited to a single connexin isoform, Cx43. However, other isoforms are known to be expressed in the AVJ of mammalian species, including Cx45, Cx40, and Cx31.9/Cx30.2. Unfortunately, we were unable to obtain antibodies to these connexins that would provide quantifiable signals in the human AVJ. Additionally, our study was based on immunohistochem istry; therefore, the detection of Cx43 was limited by the resolution of this technique. It is certainly possible that gap junctions composed of Cx43 were small enough to escape detection with immunofluorescence. Our study was conducted in human hearts that were not previously characterized in the electrophysiology lab.

Acknowledgments

Grant sponsor: American Heart Association; Grant number: 0750031Z.

LITERATURE CITED

Anderson, RH.; Ho, SY. The atrial connections of the specialized axis responsible for AV conduction. In: Mazgalev, TN.; Tchou, PJ., editors. Atrial-AV nodal electrophysiology: a view from the millenium. Futura Publishing Company; Armonk, NY: 2000. p. 3-24.

Anderson RH, Ho SY. The morphology of the specialized atrioventricular junctional area: the evolution of understanding. Pacing Clin Electrophysiol 2002;25:957–966. [PubMed: 12137349]

Anderson RH, Durrer D, Janse MJ, van Capelle FJL, Billete JACQ, Becker AE, Durrer D. A combined morphological and electrophysiological study of the atrioventricular node of the rabbit heart. Circ Res 1974;35:909–922. [PubMed: 4430083]

Billette J. Atrioventricular nodal activation during periodic premature stimulation of the atrium. Am J Physiol 1987;252:H163–H177. [PubMed: 3812708]

Billette J. What is the atrioventricular node? Some clues in sorting out its structure-function relationship. J Cardiovasc Electrophysiol 2002;13:515–518. [PubMed: 12030537]

Billinton N, Knight AW. Seeing the wood through the trees: a review of techniques for distinguishing green fluorescent protein from endogenous autofluorescence. Anal Biochem 2001;291:175–197. [PubMed: 11401292]

Boyett MR, Inada S, Yoo S, Li J, Liu J, Tellez J, Greener ID, Honjo H, Billeter R, Lei M, Zhang H, Efimov IR, Dobrzynski H. Connexins in the sinoatrial and atrioventricular nodes. Adv Cardiol 2006;42:175–197. [PubMed: 16646591]

Camelliti P, Borg TK, Kohl P. Structural and functional characterisation of cardiac fibroblasts. Cardiovasc Res 2005;65:40–51. [PubMed: 15621032]

Coppen SR, Severs NJ. Diversity of connexin expression patterns in the atrioventricular node: vestigial consequence or functional specialization? J Cardiovasc Electrophysiol 2002;13:625–626. [PubMed: 12108510]

Coppen SR, Kaba RA, Halliday D, Dupont E, Skepper JN, Elneil S, Severs NJ. Comparison of connexin expression patterns in the developing mouse heart and human foetal heart. Mol Cell Biochem 2003;242:121–127. [PubMed: 12619874]

Cosio FG, Anderson RH, Kuck KH, Becker A, Borggrefe M, Campbell RW, Gaita F, Guiraudon GM, Haissaguerre M, Rufilanchas JJ, Thiene G, Wellens HJ, Langberg J, Benditt DG, Bharati S, Klein G, Marchlinski F, Saksena S. Living anatomy of the atrioventricular junctions. A guide to electrophysiologic mapping. A consensus statement from the Cardiac Nomenclature Study Group, Working Group of Arrhythmias, European Society of Cardiology, and the Task Force on Cardiac Nomenclature from NASPE. Circulation 1999;100:e31–e37. [PubMed: 10430823]

Davis LM, Rodefeld ME, Green K, Beyer EC, Saffitz JE. Gap junction protein phenotypes of the human heart and conduction system. J Cardiovasc Electrophysiol 1995;6:813–822. [PubMed: 8542077]

Deshmukh PM, Romanyshyn M. Direct his-bundle pacing: present and future. Pacing Clin Electrophysiol 2004;27:862–870. [PubMed: 15189517]

Dobrzynski H, Nikolski VP, Sambelashvili AT, Greener ID, Yamamoto M, Boyett MR, Efimov IR. Site of origin and molecular substrate of atrioventricular junctional rhythm in the rabbit heart. Circ Res 2003;93:1102–1110. [PubMed: 14563715]

Dupont E, Matsushita T, Kaba RA, Vozzi C, Coppen SR, Khan N, Kaprielian R, Yacoub MH, Severs NJ. Altered connexin expression in human congestive heart failure. J Mol Cell Cardiol 2001;33:359–371. [PubMed: 11162139]

Goldsmith EC, Hoffman A, Morales MO, Potts JD, Price RL, McFadden A, Rice M, Borg TK. Organization of fibroblasts in the heart. Dev Dyn 2004;230:787–794. [PubMed: 15254913]

Hill AJ, Ahlberg SE, Wilkoff BL, Iaizzo PA. Dynamic obstruction to coronary sinus access: the Thebesian valve. Heart Rhythm 2006;3:1240–1241. [PubMed: 17018361]

Hucker WJ, Nikolski VP, Efimov IR. Autonomic control and innervation of the atrioventricular junctional pacemaker. Heart Rhythm 2007a;4:1326–1335. [PubMed: 17905339]

Hucker WJ, Sharma V, Nikolski VP, Efimov IR. Atrio-ventricular conduction with and without AV nodal delay: two pathways to the bundle of His in the rabbit heart. Am J Physiol Heart Circ Physiol 2007b; 293:H1122–HH1130. [PubMed: 17496219]

Inoue S, Becker AE. Posterior extensions of the human compact atrioventricular node: a neglected anatomic feature of potential clinical significance. Circulation 1998;97:188–193. [PubMed: 9445172]

Inoue S, Becker AE, Riccardi R, Gaita F. Interruption of the inferior extension of the compact atrioventricular node underlies successful radio frequency ablation of atrioventricular nodal reentrant tachycardia. J Interv Card Electrophysiol 1999;3:273–277. [PubMed: 10490485]

Katritsis DG, Becker A. The atrioventricular nodal reentrant tachycardia circuit: a proposal. Heart Rhythm 2007;4:1354–1360. [PubMed: 17905343]

Ko YS, Yeh HI, Ko YL, Hsu YC, Chen CF, Wu S, Lee YS, Severs NJ. Three-dimensional reconstruction of the rabbit atrioventricular conduction axis by combining histological, desmin, and connexin mapping data. Circulation 2004;109:1172–1179. [PubMed: 14769705]

Kreuzberg MM, Schrickel JW, Ghanem A, Kim JS, Degen J, Janssen-Bienhold U, Lewalter T, Tiemann K, Willecke K. Connexin30.2 containing gap junction channels decelerate impulse propagation through the atrioventricular node. Proc Natl Acad Sci U S A 2006;103:5959–5964. [PubMed: 16571663]

Laske TG, Skadsberg ND, Hill AJ, Klein GJ, Iaizzo PA. Excitation of the intrinsic conduction system through His and inter-ventricular septal pacing. Pacing Clin Electrophysiol 2006;29:397–405. [PubMed: 16650269]

McGuire, M. What is the slow AV nodal pathway?. In: Mazgalev, TN.; Tchou, PJ., editors. Atrial-AV nodal electrophysiology: a view from the millenium. Futura; Armonk: 2000. p. 183-197.

Medkour D, Becker AE, Khalife K, Billette J. Anatomic and functional characteristics of a slow posterior AV nodal pathway: role in dual-pathway physiology and reentry. Circulation 1998;98:164–174. [PubMed: 9679723]

Moe GK, Preston JB, Burlington H. Physiologic evidence for a dual A-V transmission system. Circ Res 1956;4:357–375. [PubMed: 13330177]

Nikolski VP, Jones SA, Lancaster MK, Boyett MR, Efimov IR. Cx43 and the dual-pathway electrophysiology of the AV node and AV nodal reentry. Circ Res 2003;92:469–475. [PubMed: 12600895]

Rothenberg F, Efimov IR. Three-dimensional anatomy of the conduction system of the early embryonic rabbit heart. Anat Rec A Discov Mol Cell Evol Biol 2006;288:3–7. [PubMed: 16287158]

Schnell SA, Staines WA, Wessendorf MW. Reduction of lipofuscin-like autofluorescence in fluorescently labeled tissue. J Histochem Cytochem 1999;47:719–730. [PubMed: 10330448]

Shaw RM, Rudy Y. Ionic mechanisms of propagation in cardiac tissue: roles of the sodium and L-type calcium currents during reduced excitability and decreased gap junction coupling. Circ Res 1997;81:727–741. [PubMed: 9351447]

Sigg DC, Hiniduma-Lokuge P, Coles JA Jr, Falkner P, Rose R, Urban JF, Ujhelyi MR. Focal pharmacological modulation of atrioventricular nodal conduction via implantable catheter: a novel therapy for atrial fibrillation? Circulation 2006;113:2383–2390. [PubMed: 16702470]

Tawara, S. Das Reizleitungssystem des Saugetierherzens: Eine Anatomische-Histologische Studie Uber Das Atrioventrikularbundel Und Die Purkinjeschen Faden. Verlag von Gustav Fischer; Jena: 1906.

Zanon F, Baracca E, Aggio S, Pastore G, Boaretto G, Cardano P, Marotta T, Rigatelli G, Galasso M, Carraro M, Zonzin P. A feasible approach for direct His-bundle pacing using a new steerable catheter to facilitate precise lead placement. J Cardiovasc Electrophysiol 2006;17:29–33. [PubMed: 16426396]

Zhang Y, Bharati S, Mowrey KA, Zhuang S, Tchou PJ, Mazgalev TN. His electrogram alternans reveal dual-wavefront inputs into and longitudinal dissociation within the bundle of His. Circulation 2001;104:832–838. [PubMed: 11502711]

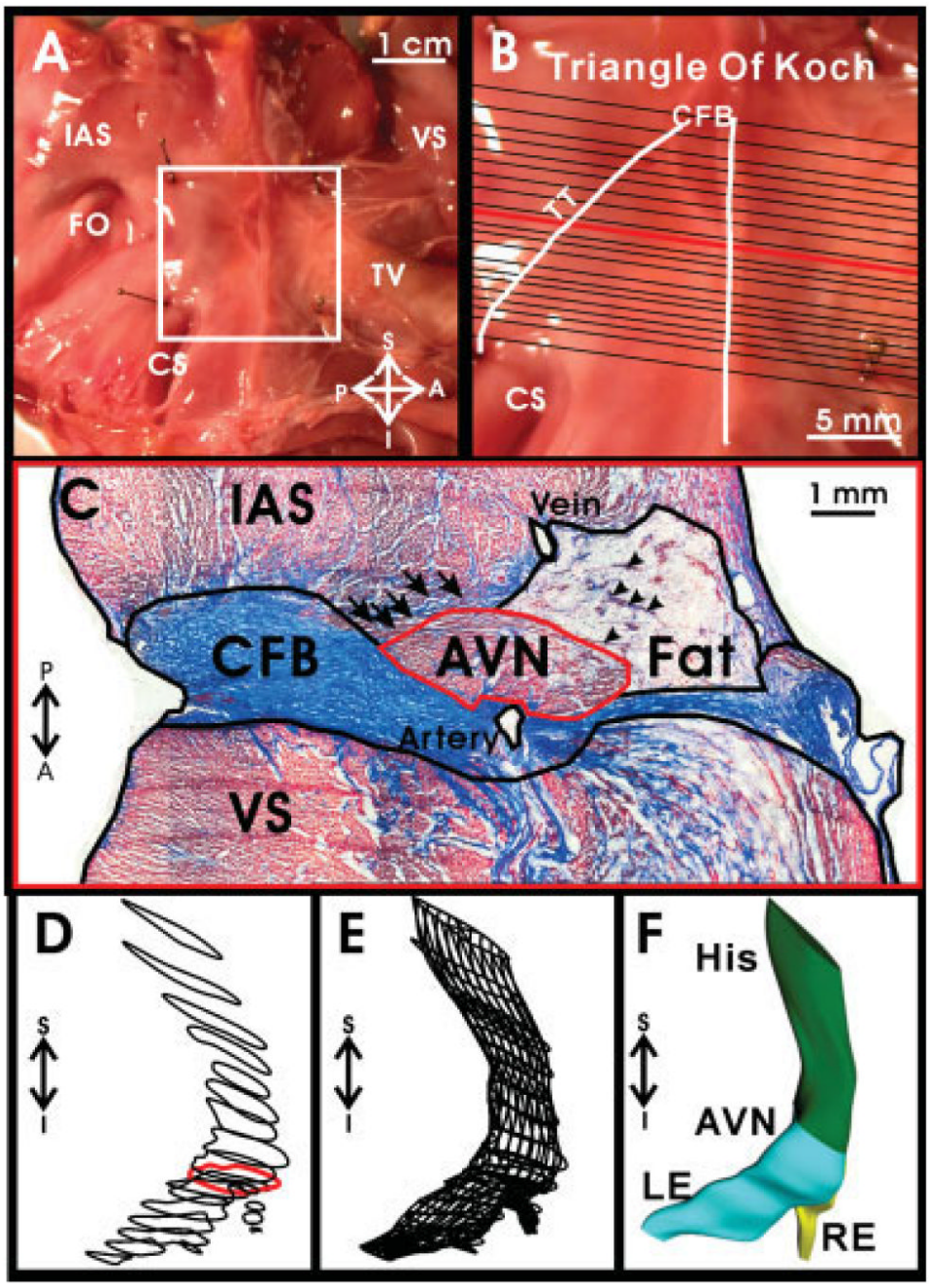

Fig. 1.

Dissection of human atrioventricular junction (AVJ) and creation of a three-dimensional (3D) reconstruction. **A:** Dissected AV junctional preparation with anatomical landmarks labeled. **B:** High-resolution image of the boxed area in A, with locations of sections stained with Masson trichrome marked. Also the triangle of Koch is outlined, which is bounded by the tendon of Todaro (TT), the coronary sinus (CS), and the septal leaflet of the tricuspid valve (TV). **C:** Masson trichrome staining of section marked by a red line in B, with different tissue areas outlined for 3D reconstruction. **D:** Outlines of the conduction system of all sections aligned in three dimensions. Red outline corresponds to the AV node outlined in C. **E:** Outlines of the conduction system lofted to create a 3D mesh. **F:** The 3D mesh in E rendered to approximate

the 3D volume. AVN, AV node; CFB, central fibrous body; FO, fossa ovalis; IAS, intraatrial septum; LE: leftward extension; RE, rightward extension; VS, ventricular septum; S,I,P,A, superior, inferior, posterior, anterior orientation.

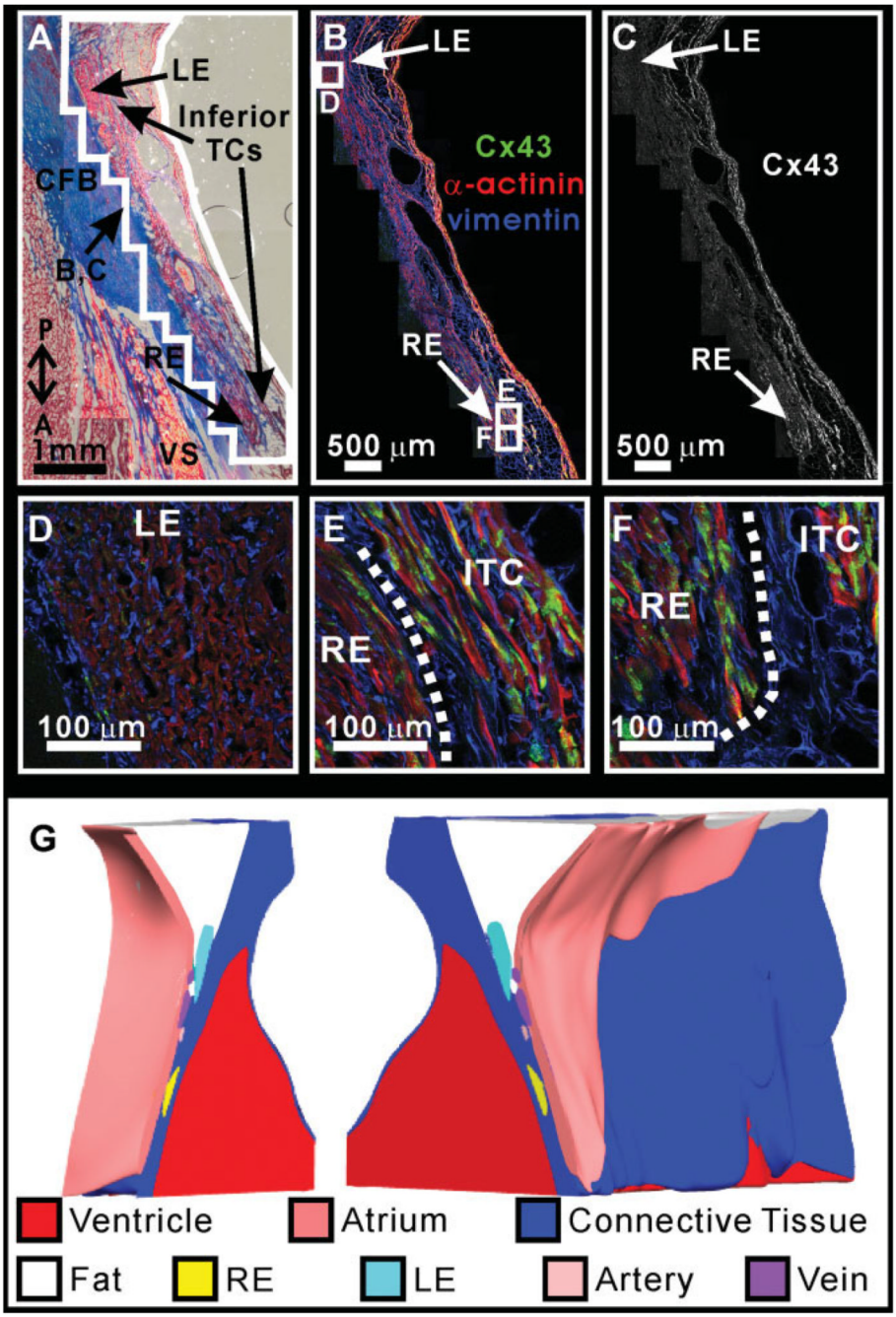

Fig. 2.

Cx43 density in the nodal extensions. **A:** Masson trichrome stain of the nodal extensions. Outlined area surrounding the nodal extensions corresponds to immunohistochemistry shown in panels B and C. **B:** Immunohistochemistry of the nodal extensions showing α-actinin in red, vimentin in blue, and Cx43 in green. **C:** Cx43 expression in the nodal extensions. **D—F:** Higher magnification of Cx43, vimentin, and α-actinin expression in leftward extension (D), the rightward extension, and the inferior transitional cells (E,F). **G:** Three-dimensional reconstruction of the atrioventricular junction (AVJ) split open at the plane of section shown in panels A—C. CFB, central fibrous body; IAS, interatrial septum; LE, leftward extension; RE, rightward extension; VS, ventricular septum; P,A, posterior—anterior orientation.

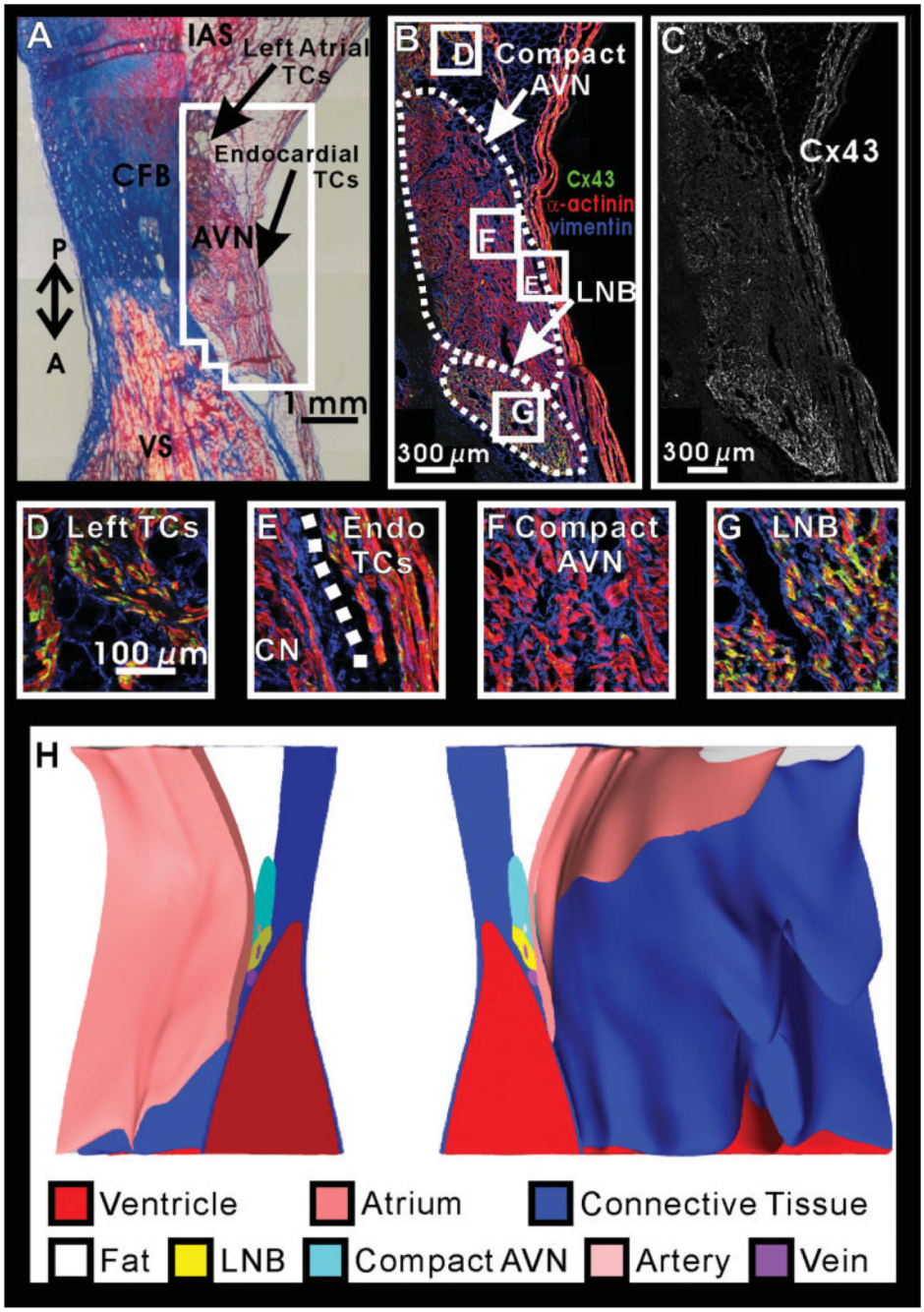

Fig. 3.

Cx43 density in the atrioventricular node (AVN). **A:** Masson trichrome stain of the AVN. Outlined area surrounding the AVN corresponds to immunohistochemistry shown in panels B and C. **B:** Immunohistochemistry of the AVN showing α-actinin in red, vimentin in blue, and Cx43 in green. **C:** Cx43 expression in the AVN. **D—G:** Higher magnification of Cx43, vimentin, and α-actinin expression in various areas of the AVN region. **H:** Three-dimensional reconstruction of the AVJ split open at the plane of section shown in A—C. CFB, central fibrous body; IAS, interatrial septum; LNB, lower nodal bundle; VS, ventricular septum; P,A, posterior—anterior orientation.

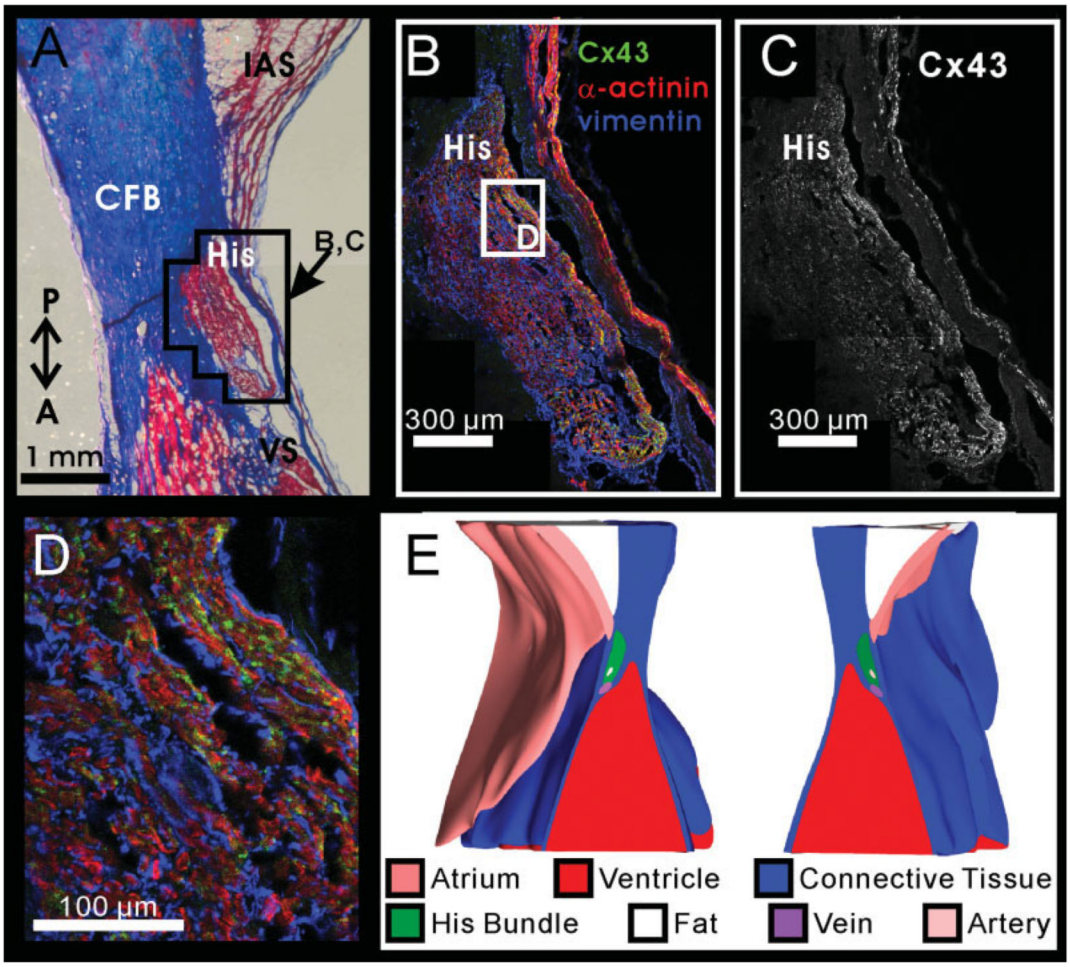

Fig. 4.

Cx43 density in the His bundle. **A:** Masson trichrome stain of the His bundle. Outlined area surrounding the His bundle corresponds to immunohistochemistry shown in B and C. **B:** Immunohistochemistry of the His bundle showing α-actinin in red, vimentin in blue, and Cx43 in green. **C:** Cx43 expression in the His bundle. **D:** Higher magnification of Cx43, vimentin, and α-actinin expression in the His bundle. **E:** Three-dimensional reconstruction of the atrioventricular junction (AVJ), which was split open at the plane of section shown in panels A—C. CFB, central fibrous body; IAS, interatrial septum; VS, ventricular septum; P,A, posterior—anterior orientation.

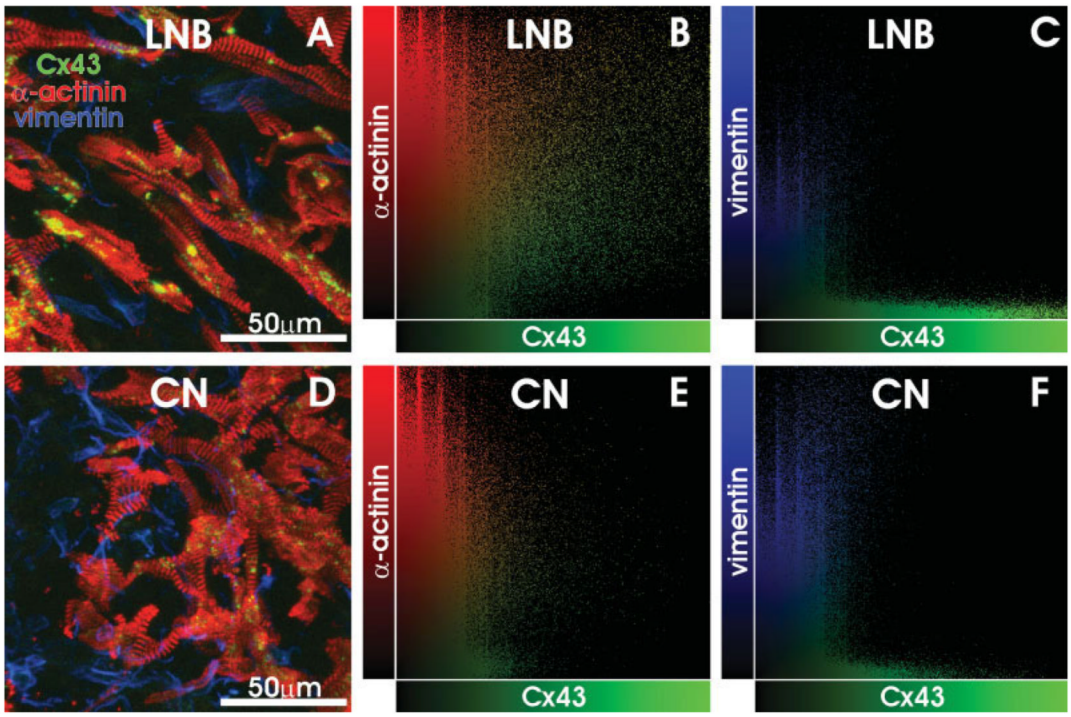

Fig. 5.

Cellular Expression of Cx43. **A:** Maximum projection image of Cx43 (green) α-actinin (red) and vimentin (blue) staining in the lower nodal bundle (LNB). **B:** Colocalization of Cx43 and α-actinin, showing that voxels of high Cx43 intensity also have a high α-actinin signal. **C:** Colocalization of Cx43 and vimentin, showing that voxels of high Cx43 intensity have no significant vimentin signal. **D,E:** Data similar to A—C for the compact node (CN). See text for details.

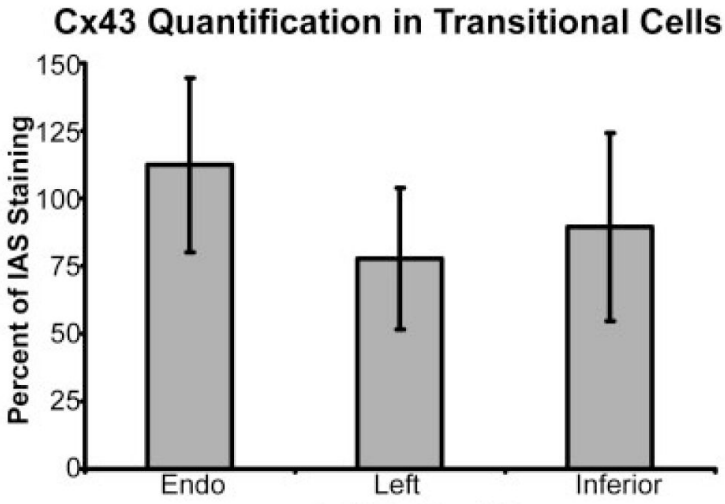

	Cx43 Staining (%)				
Heart	IAS	Endo	Left	IAS	Inferior
1	3.92	3.79	2.21	3.42	2.11
2	6.42	4.77	4.91	8.38	11.40
3	4.83	6.85	3.03	8.96	5.78
4 (DCM)	7.85	10.73	9.01	14.28	13.63
Average	**5.76**	**6.53**	**4.79**	**8.76**	**8.23**
Ratio*100		**112± 32%**	**78± 26%**		**89± 35%**

Fig. 6.

Cx43 density in transitional cells in the atrioventricular junction (AVJ). Cx43 density in the endocardial (endo), left-sided, and inferior transitional cells. All densities are normalized to the Cx43 density of the interatrial septum (IAS). DCM, dilated cardiomyopathy.

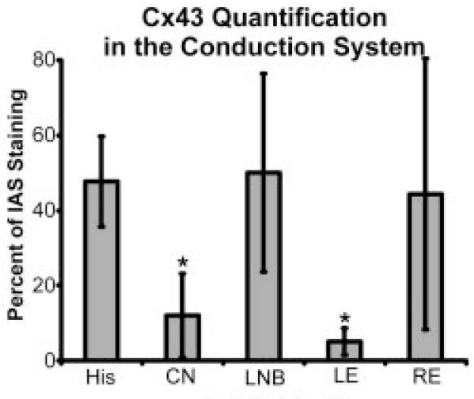

Cx43 Staining (%)

Heart	IAS	His	IAS	CN	LNB	IAS	LE	RE
1	3.42	1.68	3.92	0.153	1.44	3.42	0.209	0.97
2	4.15	2.35	6.42	0.505	5.46	8.38	0.086	3.76
3	6.59	3.61	4.83	1.377	2.61	8.96		0.91
4 (DCM)	13.47	4.08	7.85	0.609	1.91	14.28	1.124	13.42
Average	**6.91**	**2.93**	**5.76**	**0.661**	**2.86**	**8.76**	**0.473**	**4.76**
Ratio*100		**48±12%**		**12±11%**	**50±26%**		**5±4%**	**44±36%**

Fig. 7.

Cx43 density in the conduction system of the atrioventricular junction (AVJ). All densities are normalized to the Cx43 density of the interatrial septum (IAS). CN, compact atrioventricular node; DCM, dilated cardiomyopathy; LNB, lower nodal bundle; LE, leftward extension; RE, rightward extension.

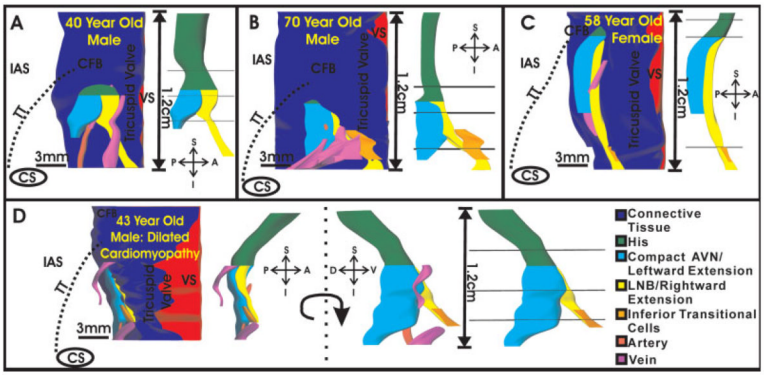

Fig. 8.

Three-dimensional reconstruction of the atrioventricular junction (AVJ) conduction system. **A—C:** Endocardial view of the conduction system of each normal heart. Left side of each panel displays the connective tissue and blood vessels surrounding the conduction system, as well as the location of the conduction system within the triangle of Koch of each preparation. Right side of each panel shows the conduction system and the three planes where Cx43 was quantified. **D:** Conduction system reconstruction of the heart with dilated cardiomyopathy. Left side of panel displays the same endocardial view as shown in A—C. Middle of panel shows the conduction system rotated 90 degrees to more clearly show leftward extension. CFB, central fibrous body; IAS, interatrial septum; TT, tendon of Todaro; VS, ventricular septum; A—P, S—I, D—V, anterior—posterior, superior—inferior, and dorsal—ventral orientations.

TABLE 1

Patient characteristics for each sample used in this study

Heart	Sex	Age	Cause of death
1	M	40	Brain tumor
2	M	70	Intercerebral hemorrhage
3	F	58	Intercerebral hemorrhage
4	M	43	Explanted: Idiopathic dilated cardiomyopathy